Modeling the structure of the ribosome

Thomas R. Easterwood and Stephen C. Harvey

Abstract: Considering the size and complexity of the ribosome and the growing body of data from a wide range of experiments on ribosomal structure, it is becoming increasingly important to develop tools that facilitate the development of reliable models for the ribosome. We use a combination of manual and computer-based approaches for building and refining models of the ribosome and other RNA–protein complexes. Our methods are aimed at determining the range of models compatible with the data, making quantitative statements about the positional uncertainties (resolution) of different regions, identifying conflicts in the data, establishing which regions of the ribosome need further experimental exploration, and, where possible, predicting the outcome of future experiments. Our previous low-resolution model for the small subunit of the *Escherichia coli* ribosome is briefly reviewed, along with progress on atomic resolution modeling of the mRNA–tRNA complex and its interaction with the decoding site of the 16S RNA.

Key words: molecular models, 30S subunit, 16S decoding site, *Escherichia coli*, tRNA–mRNA complex.

Résumé : Étant donné la dimension et la complexité du ribosome, et considérant la multitude de résultats d'expériences très variées sur la structure du ribosome, il est de plus en plus important de développer des outils pour faciliter la mise au point de modèles fiables du ribosome. Nous utilisons des approches manuelles et assistées par ordinateur pour établir et raffiner des modèles du ribosome et d'autres complexes ARN–protéines. Nos méthodes visent à déterminer la gamme de modèles conciliables avec les résultats, obtenir des données quantitatives sur les incertitudes de position (résolution) de différentes régions, identifier les conflits entre les résultats, établir quelles sont les régions du ribosome nécessitant d'autres études expérimentales et, si possible, prédire les résultats des prochaines expériences. Dans ce chapitre, nous faisons une brève revue de notre modèle à faible résolution antérieur de la petite sous-unité du ribosome de *Escherichia coli* et des progrès dans la mise au point d'un modèle à résolution atomique du complexe ARNm–ARNt et de son interaction au site de décodage de l'ARNr 16S.

Mots clés : modèles moléculaires, sous-unité 30S, site de décodage de l'ARNr 16S, *Escherichia coli*, complexe ARNm–ARNt.

[Traduit par la rédaction]

Introduction

A wide range of experimental methods have been used to probe the structure of the ribosome. Results from these experiments have been synthesized into a succession of models (Expert-Bezançon and Wollenzien 1985; Brimacombe et al. 1988, 1990; Nagano et al. 1988; Stern et al. 1988; Oakes et al. 1990; Malhotra et al. 1990; Hubbard and Hearst 1991; Malhotra and Harvey 1994).

Most of these models have been built by hand, either using physical models or manually adjusted computer graphics models. This is a suitable approach when the available data are limited and of low resolution. In recent years, however, both the quantity and the resolution of the data have increased dramatically, leading to the need for automated computer-based approaches for building and refining the models.

In this article, we describe the application of two computer programs on structural studies of the ribosome. After a discussion of the philosophy behind our approach, we briefly describe the programs and then conclude with a presentation of recent results in four areas: a low-resolution model for the complete 30S subunit of the *Escherichia coli* ribosome, a high-resolution model for the complex between mRNA and the A- and P-site tRNAs, an all-atom model for the decoding region of the 16S RNA, and docking studies on interactions between the mRNA–tRNA complex and the 16S RNA.

Received May 20, 1995. Accepted August 17, 1995.

T.R. Easterwood and S.C. Harvey.[1] Department of Biochemistry and Molecular Genetics, University of Alabama at Birmingham, Birmingham, AL 35294, U.S.A.

[1] Author to whom all correspondence should be addressed.

Overall approach to modeling the ribosome

Our approach is driven by several considerations. First, the size and complexity of the ribosome and the huge amounts of available data preclude building a detailed and accurate model for the entire 70S complex at one time. A process of model building and refinement is necessary. We use "refinement" in the same sense as in crystallography or NMR: an initial model is postulated, compared with the available structural data, and then adjusted to improve the fit to the data; several iterations may be necessary to find the optimum model. As more data become available, the model is further refined to reflect them.

Second, the methods must be able to incorporate data from

a wide variety of experiments. X-ray crystallography and NMR provide information at atomic resolution on some of the ribosomal proteins and some fragments of rRNAs. Low-resolution data come from neutron diffraction, electron microscopy, immunoelectron microscopy, DNA hybridization, electron diffraction on ordered two-dimensional arrays, phylogenetic studies, mutational analyses, chemical crosslinking, and footprinting using both chemical and enzymatic probes. Proper weighting of the data, reflecting the resolution of the underlying experiments, is essential.

Third, since there are not enough data to specify a single model, the methods should define the range of models compatible with the data. Wherever possible, quantitative statements about uncertainties in positions of the various elements of the structure should be made. (This is analogous to specifying the resolution of various parts of the model and corresponds with the calculation of temperature factors and R factors in crystallography and NMR.) Such analyses allow objective evaluations of the quality of the models and identify regions of the structure where additional experiments would provide the greatest increase in knowledge. They also allow the identification of conflicts in the experimental data.

These considerations have led us to an integrated approach at two levels. (*i*) There are parts of the ribosomal structure of sufficient importance and about which there are enough data to work at atomic resolution. If available, we can simply use a structure determined by crystallography or NMR. More commonly, we must build high-resolution models for those regions. In either case, the model specifies the positions of every atom. (*ii*) In those regions where all-atom modeling is not justified, we use low-resolution models. The reduction in detail is justified both by the size of the system and by the low- resolution of the final models, which are typically in the range of 5–15 Å (1 Å = 0.1 nm). In these models, each protein is described as a sphere of appropriate volume, and RNA structures are represented by a chain of spherical particles, one per nucleotide. The low-resolution models specify the coordinates of each phosphate group in the RNA, along with the coordinates of the center of the mass of each protein. (Proteins could also be represented by the coordinates of each alpha carbon in those cases where the structure and orientation can be specified.)

These two approaches are incorporated in the final models, which mix atomic resolution in some regions with low-resolution representations in others.

A low-resolution model for the 30S subunit has been published (Malhotra and Harvey 1994). Our more recent efforts have been aimed at modeling the mRNA–tRNA complex and its interactions with the decoding region of the 16S RNA, using an atomic representation. We are in the process of refining a hybrid model that combines atomic detail in the decoding region with low-resolution representations for the rest of the 30S subunit. Our future efforts will involve the addition of a model for the 50S subunit to this complex, followed by an ongoing process of refinement and treatment of other regions at atomic detail.

Computer approaches to building and refining models

We use two different computer programs for building models. Like many other modeling groups, we have found that the MC-SYM program (Major et al. 1991; Gautheret et al. 1993) is a very powerful tool for modeling RNAs at the all-atom level. The program has been distributed to over 50 laboratories (F. Major, personal communication). MC-SYM uses a library of hundreds of nucleotide conformations to build all-atom models that satisfy specified constraints. Constraints commonly used include interatomic (or internucleotide) distances as measured by crosslinking or fluorescence energy transfer and protection patterns from enzymatic and chemical footprinting studies. The output from MC-SYM is a collection of sets of atomic coordinates; each set represents a model that satisfies the constraints, and the full collection specifies the range of models compatible with the data. It should be emphasized that MC-SYM is not a molecular mechanics program; therefore, it does not contain an energy function for optimizing or ranking the models.

We use our in-house program, YAMMP (Tan and Harvey 1993), for refinement of all-atom models. YAMMP is a general purpose modeling package that uses methods derived from molecular mechanics (McCammon and Harvey 1987), and refinement with it is similar to procedures used for refining structures from crystallography and NMR. Standard algorithms, such as energy minimization, molecular dynamics, Monte Carlo, and simulated annealing, are available in YAMMP. For the all-atom models, the energy function combines terms from standard molecular mechanics protocols (bond stretching, bond-angle deformations, torsional rotations, and van der Waals and Coulombic interactions) with terms representing experimentally derived constraints.

YAMMP is also used for building and refining low-resolution models. The details of this method have been published in a paper where we described its application to a well-characterized test system with a known crystal structure, tRNA (Malhotra et al. 1994*a*). Briefly, for RNA models, initial random chain configurations are generated and then refined into conformations that satisfy the constraints of secondary and tertiary structure and distance constraints from crosslinking, footprinting, energy transfer, and other experiments. One unique feature of YAMMP is that it also incorporates constraints reflecting shape information from electron microscopy and positional information from immunoelectron microscopy (Malhotra et al. 1994*b*). The energy function for the low-resolution models is different from that for the all-atom models, because it has no conventional terms for covalent and nonbonded interactions and represents only experimental constraints. It has been designed so that any model that satisfies all of the constraints will have an energy of zero (a perfect score). Unsatisfied constraints will show up as positive energies so that the total energy measures the overall deviation of the model from a perfect one.

Since YAMMP is a general purpose program, it can also be used to refine the final mixed-mode models, with atomic detail in some regions and low-resolution representation in others.

Low-resolution model for the 30S subunit of the *E. coli* ribosome

We recently published models for the 30S subunit (Malhotra and Harvey 1994). In that study, the protein positions from the neutron diffraction map (Capel et al. 1988) were used, although the effects on the model of alternative positions for

S20 were also discussed and there was some movement of the proteins during refinement. About 75% of the RNA chain was localized with an uncertainty of 5–15 Å, justifying the low-resolution approach. The binding site of the tRNA–mRNA complex in the decoding region was represented by a spherical volume, but we did not believe that the data justified specification of the exact coordinates of each phosphate group in the complex.

Overall, our models resemble the manually built models (Expert-Bezançon and Wollenzien 1985; Brimacombe et al. 1988; Stern et al. 1988; Nagano et al. 1988; Oakes et al. 1990), with the 5′ and central domains clustered in the body of the 30S subunit and the 3′ domain filling the head; however, there are significant differences in the positions of some helices, particularly near the active site. These differences are discussed in detail in Malhotra and Harvey (1994).

The tRNA–mRNA complex

During peptidyl transfer, two tRNAs are simultaneously bound to the mRNA, and their 3′ termini must be in contact so that the peptide bond can be formed. There are two possible configurations for the complex between mRNA and the tRNAs. They are called R and S for the scientists who first proposed them (Rich 1974; Sundaralingam et al. 1975). The reader can visualize these two models by representing the A-site tRNA with the thumb and index finger of the left hand, keeping these at a right angle to one another, and by representing the P-site tRNA with the thumb and index finger of the right hand, in a similar conformation. The tips of the thumbs must be kept in contact, representing the juxtaposition of the two anticodons when they are bound to the mRNA. At the same time, the tips of the index fingers should be kept in contact, to represent the contact between amino acids covalently bound at the 3′ terminus of each tRNA. Several experiments have shown that the two tRNAs lie in fairly close contact across their entire L-shaped bodies. You can achieve this in two ways. One is to bring your palms together and interlace the middle, ring, and little fingers of your two hands, so that your thumbs and index fingers point toward you; this gives an S model. The other way is to bring the backs of your hands together, so that the thumbs and index fingers point away from you; this represents the R model.

Our first investigation of the complex between mRNA and two tRNAs gave an S model (Prabhakaran and Harvey 1989). A similar solution had been proposed by McDonald and Rein (1987). In more exhaustive studies, Valery Lim built both R and S models, and he and the Brimacombe group concluded that the data favor the R model (Lim et al. 1992). This surprised us because we had examined simple physical models and concluded that R models were very unfavorable on simple steric grounds. S models lay the mRNA in a fairly smooth right-handed wrapping around the anticodon regions of the two tRNAs, while R models leave the 5′ end of the mRNA buried between the two tRNAs, requiring a very sharp reversal of the backbone to prevent tangling during the translocation step.

Therefore, we decided to independently build both R and S models and to reassess Lim's models. We found that S models could be built quite easily with MC-SYM, but the program did not produce a single R model. While this was compatible with the conclusion that we had drawn using physical models, it could not rigorously rule out R models. As a result, we compared distances in the R and S models of Lim et al. (1992), and in our own S models, with the available experimental data.

Fig. 1. The heart of the 16S rRNA decoding site. The 1400–1500 sequence from *E. coli* is shown with — indicating canonical Watson–Crick base pairs and • indicating noncanonical base pairs (Gutell et al. 1994). The A and P sites as determined by protection–modification experiments are also indicated.

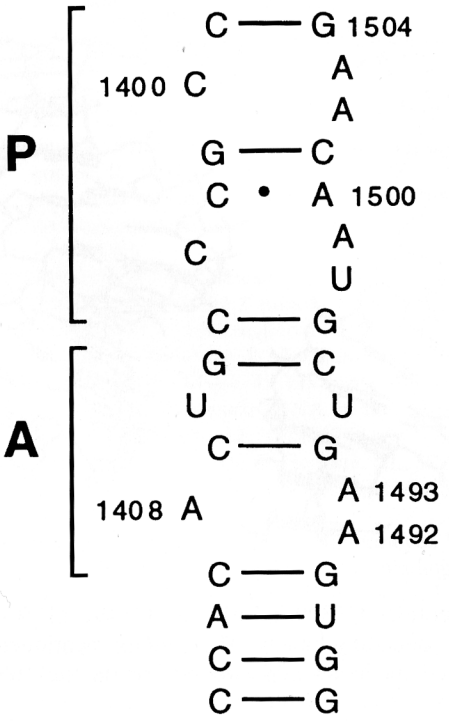

Distances within the tRNA–mRNA complex have been measured by fluorescence energy transfer (Johnson et al. 1982; Paulsen et al. 1983) and by chemical crosslinking (Odom et al. 1978; Fairclough et al. 1979). We found that only the S model is compatible with those distances and that it is further favored by two steric considerations, one arising from an observed photocrosslink between nucleotide 34 of the P-site tRNA and residue C1400 of the 16S RNA (Prince et al. 1982; Ciesiolka et al. 1985; Gornicki et al. 1985) and the other explaining the effects of substitutions in the anticodon loop of the P-site tRNA on the binding of tRNA at the A site (Smith & Yarus 1989). Details of this study are described in Easterwood et al. (1994). It is also worth noting that the Brimacombe group now agrees that S models are favored (Rinke-Appel et al. 1994).

The decoding site

The decoding function of the ribosome falls primarily to the small ribosomal subunit. In the *E. coli* 30S subunit, the 16S ribosomal RNA contains a highly conserved sequence in the 1400–1500 region (Gutell et al. 1994). Many chemical and enzymatic probing studies on this region (Douthwaite et al. 1983; Van Stolk and Noller 1984; Moazed et al. 1986; Moazed and Noller 1986, 1990) as well as crosslinking studies (Prince et al. 1982; Gornicki et al. 1984, 1985; Ciesiolka et al. 1985; Brimacombe et al. 1993; Döring et al. 1994) and mutational experiments (Cunningham et al. 1992, 1993) have dem-

Fig. 2. Stereo triple of the model for the decoding region of the 16S RNA. The P site (including C1400) is located at the top of the structure in this view, the A site is in the central region, and a four base pair helix completes the bottom of the molecule. The left pair of images will give correct stereo when viewed with stereo glasses (walleyed view), while the right pair will produce a correct image when viewed with crossed eyes.

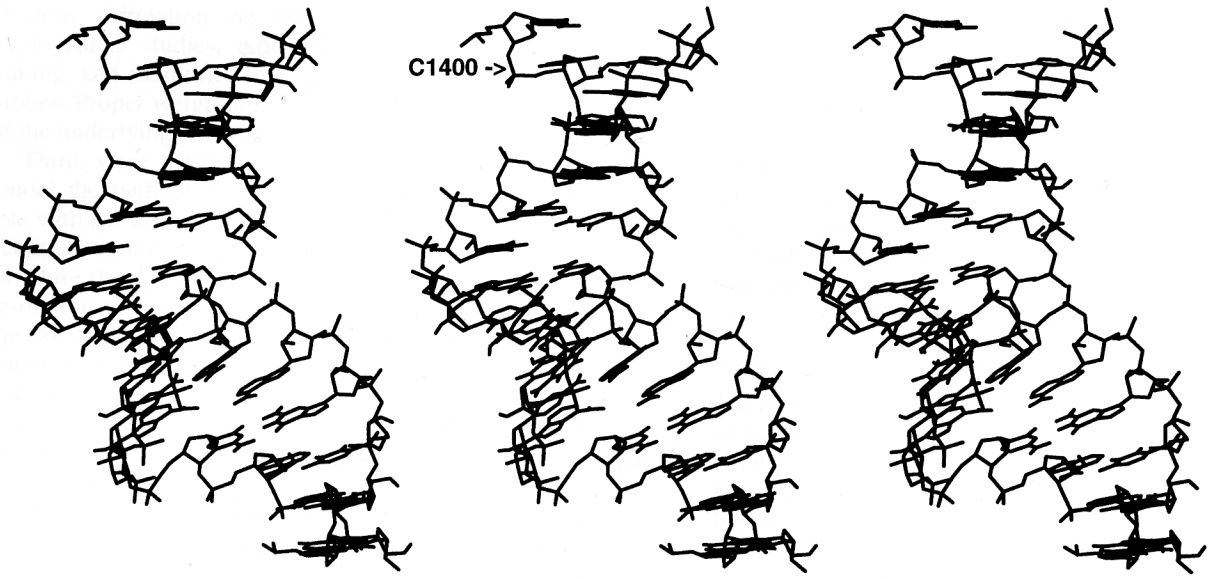

onstrated that nucleotides C1399–C1409 and G1492–G1504 are the heart of the decoding center. The studies mentioned here were performed on intact 30S subunits or on the 16S rRNA alone.

A more recent series of experiments performed by Purohit and Stern (1994) demonstrate that this 1400–1500 decoding segment of the 16S rRNA, when extracted from the rest of the 16S rRNA, can bind antibiotics with similar protection patterns as in the intact 16S rRNA. Purohit and Stern were also able to show that the segment could bind tRNA anticodon stem–loop analogues and poly(U) mRNA analogues and provide similar protection patterns as in the intact 16S rRNA. The implications of the Purohit and Stern experiments is that the heart of the decoding site has a stable structure.

All of the experimental information taken together indicate that the 1400–1500 region accommodates the tRNAs and mRNA of the translation complex into the major groove of the 1400–1500 region. The presence of several canonical and noncanonical pairings, summarized in Gutell et al. (1994) and shown in Fig. 1, begins to give a definite structure to this region once considered to be mostly single stranded. The compilation of the above information has allowed us to begin modeling the 1400–1500 decoding region at all-atom resolution, using MC-SYM. The large number of bilateral, asymmetric bulges in this region led us to visually select the structures with broader major grooves, as indicated by probing experiments of this region (Douthwaite et al. 1983) and studies on bulges and major-groove accessibility in other molecules (Weeks and Crothers 1993). The models produced by MC-SYM incorporate base pairings, both canonical and noncanonical, and information from chemical probing experiments.

Figure 2 provides an illustration of one of our models after refinement using the Tripos force field. One of the more interesting aspects of the A site is that it is somewhat smaller than the P site. The reason for this is the presence of short, four base pair helical regions bordering the A1408, A1492, and A1493 bilateral asymmetric bulge. The A site has been implicated from several studies to interact with the mRNA, specifically with the ribose–phosphate backbone (Purohit and Stern 1994). The single bilateral asymmetric bulge allows the major groove to open just wide enough to accept the ribose–phosphate backbone of an mRNA strand.

The P site of this region consists of two bilateral asymmetric bulges separated by a canonical G1401:C1501 and a noncanonical C1403:A1500 pair. As a result of the tandem bulges, the P-site region has an extremely open major groove, allowing for many interactions. The lack of a helical region immediately beyond the P site also leaves the area open for various molecular interactions. This region has been noted for binding the P-site tRNA, and the wide, open major groove would allow such an interaction.

The initial docking of our tRNA–mRNA complex into the minimized 1400–1500 decoding model from MC-SYM provides several insights into the action and properties of the decoding site. The primary interaction of the A site appears to be with the mRNA only. In the P site, the primary interaction appears to be with the tRNA. These initial insights are well explained by the following observations from the literature.

The focus of the A site region appears to be on the correct presentation of the base-pairing face of the mRNA codon. Studies have indicated that the ribose–phosphate backbone of the mRNA interacts with the base-pairing face of the As in this region (Purohit and Stern 1994), and the narrowing of the A-site major groove may facilitate holding the mRNA in the correct orientation to present the base-pairing face of the codon to the tRNA anticodon. In addition, this holding effect of the A-site region would emphasize the base pairing between codon and anticodon and thus lead to enhancement of messenger decoding. Also, the narrowness of the groove and the presentation of the base-pairing face of the mRNA would explain the

observation that tRNA protections in the A site are primarily mRNA dependent (Moazed and Noller 1986).

The focus of the P site of the decoding region seems to be on holding the tRNA with the polypeptide until the next aminoacyl tRNA arrives and polypeptide chain transfer can occur. The P site of the decoding region has been noted for binding tRNAs, even in the absence of message. The protection of N7 of G1401 by the P site bound tRNA (Moazed and Noller 1990) indicates that the tRNA is bound to the major-groove side of this region. The crosslink of U34 of the P site bound tRNA to C1400 in a UV dimer conformation (Prince et al. 1982) also indicates that the tRNA is bound in the major groove in the P site, since the 5–6 double bond of C1400 involved in the UV dimerization faces the major groove. The myriad of possible interactions in the major groove would enhance the binding of the tRNA in the P site, holding it in position for initiation and (or) elongation steps. This explains the observation that the P-site protections and thus binding of tRNA is not mRNA dependent (Moazed and Noller 1986). The P site of the decoding region seems to hold the tRNA in place, which is reasonable since the tRNA at this position holds the object of most importance, the growing polypeptide chain.

We have begun docking the tRNA–mRNA–16S decoding region onto our low-resolution model of the 30S subunit (Malhotra and Harvey 1994). Minor adjustment to our model for the 16S RNA was required in the immediate vicinity of the decoding region. The 3′ termini of the two tRNAs are juxtaposed and face the 50S subunit as required, but the exact orientation cannot be specified until we complete a model for the 50S subunit.

The combination of careful manual model building and automated computer procedures allows the development and refinement of ribosomal models. The computer methods guarantee that successive adjustments yield models that agree with all the available data, something that is extremely difficult in the absence of suitable refinement programs. All-atom detail can be used in regions where structures have been determined by crystallography or NMR or in areas where importance justifies speculation at atomic resolution. Less important or less well-defined regions are modeled at low resolution. The first details of the decoding site are beginning to emerge, and we are entering a very exciting phase of structural studies on the ribosome.

References

Brimacombe, R., Atmadja, J., Stiege, W., and Schüler, D. 1988. A detailed model of the three-dimensional structure of *Escherichia coli* 16S ribosomal RNA in situ in the 30S subunit. J. Mol. Biol. **199**: 115–136.

Brimacombe, R., Gornicki, P., Greuer, B., Mitchell, P., Osswald, M., Rinke-Appel, J., Schüler, D., and Stade, K. 1990. The three-dimensional structure and function of *Escherichia coli* ribosomal RNA, as studied by cross-linking techniques. Biochim. Biophys. Acta, **1050**: 8–13.

Brimacombe, R., Mitchell, P., Osswald, M., Stade, K., and Bochkariov, D. 1993. Clustering of modified nucleotides at the functional center of bacterial ribosomal RNA. FASEB J. **7**: 161–167.

Capel, M.S., Kjelgaard, M., Engelman, D.M., and Moore, P.B. 1988. Positions of S2, S13, S16, S17, S19 and S21 in the 30S ribosomal subunit of *E. coli*. J. Mol. Biol. **200**: 65–87.

Ciesiolka, J., Gornicki, P., and Ofengand, J. 1985. Identification of the site of cross-linking in 16S rRNA of an aromatic azide photoaffinity probe attached to the 5′-anticodon base of a site bound tRNA. Biochemistry, **24**: 4931–4938.

Cunningham, P.R., Nurse, K., Weitzmann, C.J., Négre, D., and Ofengand, J. 1992. G1402: a keystone nucleotide at the decoding site of *Escherichia coli* 30S ribosomes. Biochemistry, **31**: 7629–7637.

Cunningham, P.R., Nurse, K., Weitzmann, C.J., and Ofengand, J. 1993. Functional effects of base changes which further define the decoding center of *Escherichia coli* 16S ribosomal RNA: mutation of C1404, G1405, C1496, G1497, and U1498. Biochemistry, **32**: 7172–7180.

Döring, T., Mitchell, P., Osswald, M., Bochkariov, D., and Brimacombe, R. 1994. The decoding region of 16S RNA: a cross-linking study of the ribosomal A, P and E sites using tRNA derivatized at position 32 in the anticodon loop. EMBO J. **13**: 2677–2685.

Douthwaite, S., Christensen, A., and Garrett, R.A. 1983. Higher order structure in the 3′ minor domain of small subunit ribosomal RNAs from a gram negative bacterium, a gram positive bacterium and a eukaryote. J. Mol. Biol. **169**: 249–279.

Easterwood, T.R., Major, F., Malhotra, A., and Harvey, S.C. 1994. Orientations of transfer RNA in the ribosomal A and P sites. Nucleic Acids Res. **22**: 3779–3786.

Expert-Bezançon, A., and Wollenzien, P.L. 1985. Three-dimensional arrangement of the *Escherichia coli* 16S ribosomal RNA. J. Mol. Biol. **184**: 53–66.

Fairclough, R.H., Cantor, C.R., Wintermeyer, W., and Zachau, H.G. 1979. Fluorescence studies of the binding of a yeast $tRNA^{Phe}$ derivative to *Escherichia coli* ribosomes. J. Mol. Biol. **132**: 557–573.

Gautheret, D. Major, F., and Cedergren, R. 1993. Modeling the three-dimensional structure of RNA using discrete nucleotide conformational sets. J. Mol. Biol. **229**: 1049–1064.

Gornicki, P., Nurse, K., Hellmann, W., Boublik, M., and Ofengand, J. 1984. High resolution localization of the tRNA anticodon interaction site on the *Escherichia coli* 30S ribosomal subunit. J. Biol. Chem. **259**: 10 493 – 10 498.

Gornicki, P., Ciesiolka, J., and Ofengand, J. 1985. Cross-linking of the anticodon of P and A site bound tRNAs to the ribosome via aromatic azides of variable length: involvement of 16S rRNA at the A site. Biochemistry, **24**: 4924–4930.

Gutell, R.R., Larsen, N., and Woese, C.R. 1994. Lessons from an evolving rRNA: 16S and 23S rRNA structures from a comparative perspective. Microbiol. Rev. **58**: 10–26.

Hubbard, J.M., and Hearst, J.E. 1991. Computer modeling 16S ribosomal RNA. J. Mol. Biol. **221**: 889–907.

Johnson, A.E., Adkins, H.J., Matthews, E.A., and Cantor, C.R. 1982. Distance moved by transfer RNA during translocation from the A site to the P site on the ribosome. J. Mol. Biol. **156**: 113–140.

Lim, V., Venclovas, C., Spirin, A., Brimacombe, R., Mitchell, P., and Müller, F. 1992. How are tRNAs and mRNA arranged in the ribosome? An attempt to correlate the stereochemistry of the tRNA–mRNA interaction with constraints imposed by the ribosomal topography. Nucleic Acids Res. **20**: 2627–2637.

Major, F., Turcotte, M., Gautheret, D., Lapalme, G., Fillion, E., and Cedergren, R. 1991. The combination of symbolic and numerical computation for three-dimensional modeling of RNA. Science (Washington, D.C.), **253**: 1255–1260.

Malhotra, A., and Harvey, S.C. 1994. A quantitative model of the *Escherichia coli* 16S RNA in the 30S ribosomal subunit. J. Mol. Biol. **240**: 308–340.

Malhotra, A., Tan, R.K.Z., and Harvey, S.C. 1990. Prediction of the three-dimensional structure of the *Escherichia coli* 30S ribosomal subunit: a molecular mechanics approach. Proc. Natl. Acad. Sci. U.S.A. **87**: 1950–1954.

Malhotra, A., Tan, R.K.Z., and Harvey, S.C. 1994*a*. Modeling large RNAs and ribonucleoprotein particles using molecular mechanics techniques Biophys. J. **66**: 1777–1795.

Malhotra, A., Tan, R.K.Z., and Harvey, S.C. 1994*b*. Utilization of shape data in molecular mechanics using a potential based on spherical harmonic surfaces. J. Comp. Chem. **15**: 191–199.

McCammon, J.A., and Harvey, S.C. 1987. Dynamics of proteins and nucleic acids. Cambridge University Press, London.

McDonald, J.J., and Rein, R. 1987. A stereochemical model of the transpeptidation complex. J. Biomol. Struct. & Dyn. **4**: 729–744.

Moazed, D., and Noller, H.F. 1986. Transfer RNA shields specific nucleotides in 16S ribosomal RNA from attack by chemical probes. Cell, **47**: 985–994.

Moazed, D., and Noller, H.F. 1990. Binding of tRNA to the ribosomal A and P sites protects two distinct sets of nucleotides in 16S rRNA. J. Mol. Biol. **211**: 135–145.

Moazed, D., Van Stolk, B.J., Douthwaite, S., and Noller, H.F. 1986. Interconversion of active and inactive 30S ribosomal subunits is accompanied by a conformational change in the decoding region of 16S rRNA. J. Mol. Biol. **191**: 483–493.

Nagano, K., Harel, M., and Takezawa, M. 1988. Prediction of the three-dimensional structure of *Escherichia coli* ribosomal RNA. J. Theor. Biol. **134**: 199–256.

Oakes, M.I., Kahan, L., and Lake, J.A. 1990. DNA-hybridization electron microscopy: tertiary structure of 16S rRNA. J. Mol. Biol. **211**: 907–918.

Odom, O.W., Craig, B.B., and Hardesty, B.A. 1978. The conformation of the anticodon loop of yeast $tRNA^{Phe}$ in solution and on ribosomes. Biopolymers, **17**: 2909–2931.

Paulsen, H., Robertson, J.M., and Wintermeyer, W. 1983. Topological arrangement of two transfer RNAs on the ribosome: fluorescence energy transfer measurements between A and P site-bound $tRNA^{Phe}$. J. Mol. Biol. **167**: 411–426.

Prabhakaran, M., and Harvey, S.C. 1989. Models for two tRNAs bound to successive codons on mRNA on the ribosome. J. Biomol. Struct. & Dyn. **7**: 167–179.

Prince, J.B., Taylor, B.H., Thurlow, D.L., Ofengand, J., and Zimmerman, R.A. 1982. Covalent crosslinking of $tRNA^{Val}$ to 16S RNA at the ribosomal P site: identification of crosslinked residues. Proc. Natl. Acad. Sci. U.S.A. **79**: 5450–5454.

Purohit, P., and Stern, S. 1994. Interactions of a small RNA with antibiotic and RNA ligands of the 30S subunit. Nature (London), **370**: 659–662.

Rich, A. 1974. How transfer RNA may move inside the ribosome. *In* Ribosomes. *Edited by* M. Nomura. Cold Spring Harbor Laboratory, New York. pp. 871–884.

Rinke-Appel, J., Junke, N., Brimacombe, R., Lavrik, I., Dokudovskaya, S., Dontsova, O., and Bogdanov, A. 1994. Contacts between 16S ribosomal RNA and mRNA within the spacer region separating the AUG codon and the Shine–Dalgarno sequence: a site-directed crosslinking study. Nucleic Acids Res. **22**: 3018–3025.

Smith, D., and Yarus, M. 1989. tRNA–tRNA interactions within cellular ribosomes. Proc. Natl. Acad. Sci. U.S.A. **86**: 4397–4401.

Stern, S., Weiser, B., and Noller, H.F. 1988. Model for the three-dimensional folding of 16S ribosomal RNA. J. Mol. Biol. **204**: 447–481.

Sundaralingam, M., Brennan, T., Yathindra, N., and Ichikawa, T. 1975. Stereochemistry of mRNA–tRNA interaction on the ribosome during peptide bond formation. *In* Structure and conformation of nucleic acids and protein–nucleic acid interactions. *Edited by* M. Sundaralingam and S.T. Rao. University Park Press, Baltimore. pp. 101–115.

Tan, R.K.Z., and Harvey, S.C. 1993. Yammp: development of a molecular mechanics program using the modular programming method. J. Comp. Chem. **14**: 455–470.

Van Stolk, B.J., and Noller, H.F. 1984. Chemical probing of conformation in large RNA molecules: analysis of 16S ribosomal RNA using diethylpyrocarbonate. J. Mol. Biol. **180**: 151–177.

Weeks, K., and Crothers, D.M. 1993. Major groove accessibility of RNA. Science (Washington, D.C.), **261**: 1574–1577.